Fourier Transform Infrared Linked Analysis of Conformational Changes in Annexin V upon Membrane Binding†

Loraine Silvestro‡ and Paul H. Axelsen*,‡,§

Department of Pharmacology, Department of Medicine, Infectious Diseases Section, and Johnson Foundation for Molecular Biophysics, University of Pennsylvania, Philadelphia, Pennsylvania 19104

Received May 29, 1998; Revised Manuscript Received October 14, 1998

ABSTRACT: Annexins are ubiquitous cellular proteins of unknown primary function that bind to anionic phospholipid membranes in a calcium-dependent manner. Correlative studies involving X-ray crystallography and electron microscopy suggest that annexins undergo a structural change upon binding to supported lipid monolayer membranes. In this investigation, novel spectroscopic and analytical techniques have been applied to verify and characterize this change. Soluble annexin V was examined with ordinary transmission infrared spectroscopy, while membrane-bound annexin V was examined with both transmission and internal reflection infrared spectroscopy. Spectra were processed by linked analysis, whereby multiple spectra are fit simultaneously with component bands that are constrained to share common fitting parameters. This approach is shown to enhance the sensitivity and accuracy of the bandfitting procedure. Our results are consistent with the general mode of membrane binding inferred from electron microscopy studies, and they provide independent support for the conclusion that annexin V undergoes a conformational change upon binding to lipid monolayer membranes. Most likely, this change involves the formation of new β structure in which interstrand hydrogen bonds orient parallel to the membrane surface.

Annexins comprise a family of structurally homologous proteins that bind to phospholipid membranes in a calcium-dependent manner. A diverse array of cellular functions have been attributed to members of this family, including the regulation of inflammation, coagulation (via lipid sequestration), exocytosis, and voltage-gated Ca^{2+} ion channel activity (*1*−*5*). However, a definitive cellular role remains to be established.

Crystal structures for several annexins have been determined, revealing a core tetrad of domains (except for annexin VI, which is an octet) each containing 5 helices connected by short coil segments, and calcium ions all bound to one aspect of the molecule (*6*−*14*). Although the stoichiometry of calcium ion binding in vivo is not definitively established, it is clear from studies of the annexins with electron microscopy that the protein surface which coordinates calcium ions is the aspect which binds the phospholipid membrane (*15*−*18*).

Examination of the crystal structure (for rat annexin V, Brookhaven entry 2RAN) indicates that a plane defined by the four Ca^{2+} ions in domains I/IV, and one defined by the three Ca^{2+} ions in domains II/III, make an angle of 37.5° with each other (Figure 1A). The aforementioned electron microscopy studies suggest that the calcium binding sites become coplanar when the protein binds to a membrane and thereby imply that some reorientation of these domains must occur. Rotation of these domains *en block* to make the seven calcium ions coplanar would require more than isolated conformational changes in residues 84/85 and 244/245 (the segments joining the helices in domains I/II and III/IV, respectively), because there are bulky side chains on the protein that preclude their close approximation (Figure 1b). This suggests that at least two of the helices in the crystal structure of annexin V must partially unwind when the protein binds to a membrane.

We have applied both transmission infrared spectroscopy and polarized attenuated total internal reflectance−Fourier transform infrared (PATIR−FTIR) spectroscopy to verify and characterize conformational changes in annexin V upon membrane binding. These approaches yield complementary information, with the transmission technique providing information about the soluble form and the internal reflection technique providing information about the membrane-bound form. Other investigators have shown that these techniques can yield virtually identical protein spectra (*19*), so that different spectroscopic results should truly represent differences in conformation.

In this paper, we also introduce linked analysis for bandfitting infrared absorption spectra. Borrowing from the principles used for the global analysis of fluorescence intensity decays (*20*, *21*), linked analysis is a means to enhance the information content of parameters recovered in the course of bandfitting infrared spectra. This is accomplished by simultaneously fitting multiple spectra and constraining selected fitting parameters to be identical across

† P.H.A. is supported by Grant GM54617 and by a grant-in-aid from the American Heart Association. L.S. is supported by NIH 5-T32GM7229.

* Address correspondence to this author at the Department of Pharmacology, University of Pennsylvania, 3620 Hamilton Walk, Philadelphia, PA 19104-6084. Tel 215-898-9238; Fax: 215-573-2236; email: axe@pharm.med.upenn.edu.

‡ Department of Pharmacology.

§ Department of Medicine, Infectious Diseases Section, and Johnson Foundation for Molecular Biophysics.

10.1021/bi981289o CCC: $18.00
Published on Web 12/08/1998

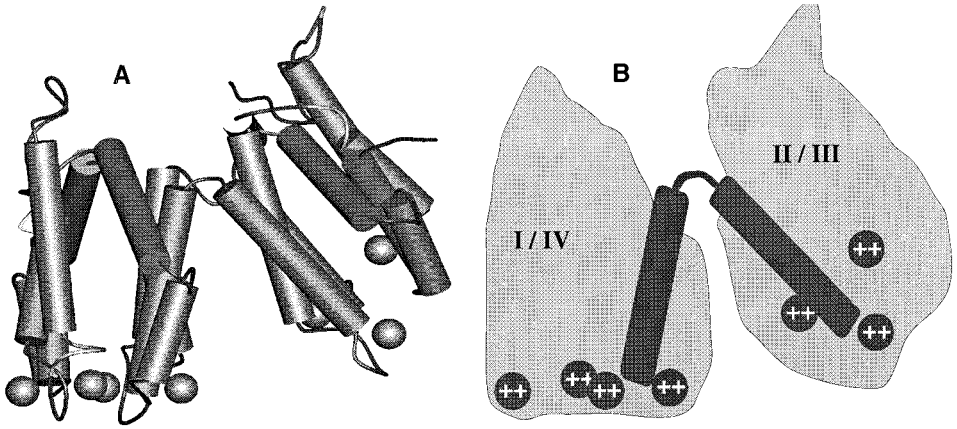

FIGURE 1: Molecular and schematic models of rat annexin V, Brookhaven structure entry 2RAN (*11*). (A) Crystal structure viewed from the intersection of a plane defined by the four calcium ions (spheres) in domains I and IV and the plane separating the domain pairs. There is a two-residue segment spanning this plane and connecting helices in domains I and II, and another two-residue segment connecting helices in domains III and IV. (B) Schematic version of the structure profile indicating the extent to which the side chains occupy space between the domains.

all the spectra being considered. We show, by means of demonstration, that linked analysis offers better accuracy and sensitivity than standard bandfitting procedures.

MATERIALS AND METHODS

Materials. Wild-type recombinant rat annexin V (2 mg/mL in 30 mM Hepes, pH 7.4) was a gift from Barbara Seaton (Boston University). Subphase buffer for internal reflection spectroscopy consisted of 30 mM Hepes in D_2O at pD 7.4. Dimyristoylphosphatidylcholine (DMPC) and dimyristoylphosphatidylserine (DMPS) in $CHCl_3$ were obtained from Avanti Polar Lipids (Alabaster, AL). Lipid concentrations were assayed by phosphate determination (*22*), and mixtures of 1:1 (mol:mol) DMPC:DMPS were prepared in 90% *n*-hexane/10% ethanol for monolayer studies. Large unilamellar vesicles composed of 80 mol % DMPC and 20 mol % DMPS were prepared in 30 mM Hepes and 2 mM $CaCl_2$ in D_2O (pD 7.4) by extrusion through a 100 nm membrane for transmission spectroscopy.

Transmission Spectroscopy. A 100 μL sample of annexin V stock in buffer was evaporated under vacuum and resuspended in 50 μL of 2 mM $CaCl_2$ in D_2O. Aliquots (80 μg of protein in 20 μL) of this solution were placed between CaF_2 windows with a 0.012 mm Teflon spacer at room temperature. A 30-fold molar excess of lipid as large unilamellar vesicles was added to selected samples. Single beam spectra (512 co-added interferograms) of samples ($\pm$ lipid) and buffer ($\pm$ lipid) were collected at 2 cm^{-1} resolution with triangular apodization and one level of zero filling, on a Bio-Rad FTS 60A FTIR spectrometer purged with dry air and equipped with a liquid nitrogen-cooled MCT detector. Absorbance spectra were obtained from the negative logarithm of the ratio of detector response for sample and buffer. Baseline correction of the absorbance spectra was performed by straight-line interpolation between spectral points at 1800 and 1590 cm^{-1}, but no smoothing or water vapor subtraction was performed on the spectra.

Internal Reflection Spectroscopy. Supported lipid monolayers, compressed to a surface pressure of 25 dyn/cm, were prepared on a silane-treated 50 $\times$ 10 $\times$ 2 mm germanium crystal with a Langmuir trough as previously described (*23*), but modified so that the crystal is applied flat onto the monolayer at the air−water interface (Figure 2). The angle of incidence between the IR beam and the crystal surface is 45° (compared to a critical angle for internal reflection of 19°). Single-beam spectra (1024 interferograms) with the polarizer oriented parallel and perpendicular to the plane of incidence were collected at room temperature before and after the injection of 20 μg of protein into the buffer subphase. The subphase buffer is stirred and has a volume of approximately 6 mL. Therefore, the membrane is exposed to a protein concentration of approximately 94 nM. As is typical for this technique, baseline correction, smoothing, and water vapor subtraction were not necessary and were not performed on these spectra.

LINKED ANALYSIS

Spectra were fit by using the FORTRAN program IRfit on a UNIX workstation. This program was adapted from Efit written earlier for global analysis of multiexponential fluorescence intensity decays (*21*). In IRfit, each spectrum is fit with one straight and level baseline and one or more bands. Each band is specified by four parameters, frequency, amplitude, full width at half-maximum (FWHM), and shape (% Gaussian, remainder = Lorentzian); initial values for each parameter must be selected. The program then adjusts the values of these parameters by means of the downhill simplex method (*24*) to achieve minimum least-squares residuals. The program, which runs on an SGI workstation under Irix 6.2, is available by contacting the corresponding author.

The unique and most important features of IRfit are that multiple bands may be fit simultaneously and that parameters in different spectra may be linked (i.e., shared, or constrained to the same value). The aim of "linked analysis" is to exploit the reasonable expectation that changing the polarization of a spectrum will change the relative amplitudes of component bands but it should not change their frequency, width, or shape. These parameters should also remain unchanged in repetitions of the same spectral measurement. Thus, linked analysis reduces the number of independent fitting parameters being applied to the available data (increasing the ratio of data to fitting parameters), and it increases the information content of each parameter by overdetermining its value. As a consequence, the likelihood of arriving at a unique fitting

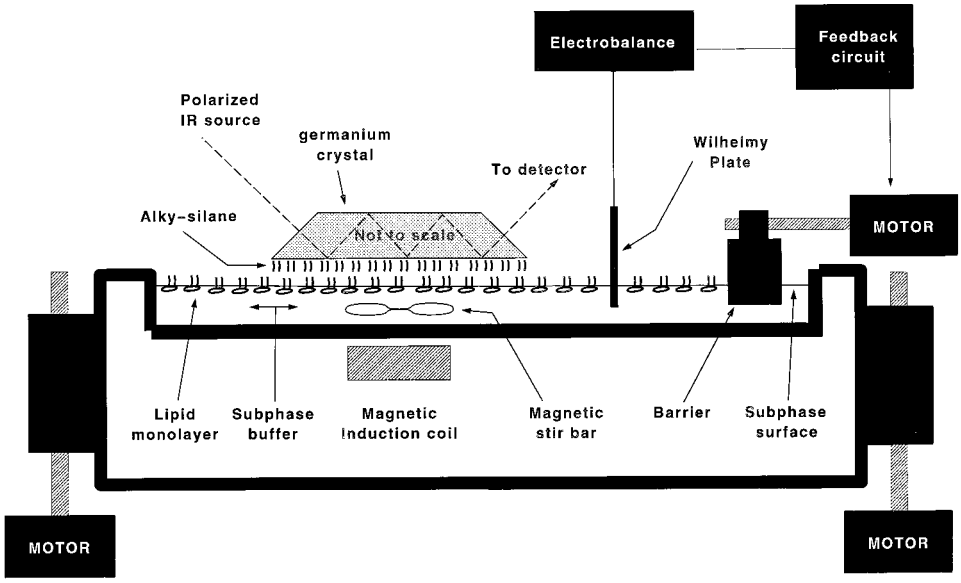

FIGURE 2: Schematic of the PATIR−FTIR spectrometer is coupled to the Langmuir trough. A silane-treated 52 × 10 × 2 mm germanium crystal is fixed in a horizontal position such that a polarized infrared beam from an FTIR spectrometer may be directed into one of its 45° end-facets and collected out of the other. In this configuration, the beam makes an angle of 45° with the surface normal and internally reflects 11 times on the upper surface and 12 times on the lower surface before exiting through the other 45° end-facet. A lipid monolayer is formed at the air−water interface, compressed to a selected pressure, and applied to the crystal surface by raising it up to the horizontally positioned crystal. Samples are introduced into the continuously stirred subphase by needle injection through the monolayer.

Table 1[a]

band	frequency (cm^{-1})	FWHM (cm^{-1})	shape % Gaussian	amplitudes (% total area)		dichroic ratio	transition order
transmission (no lipid, $n = 3$)							
1	1652.3	49.0	93.3	99.5 (0.5)			
2	1691.3	28.4	82.8	0.5 (0.5)			
internal reflection (monolayer, $n = 3$)				∥	⊥		
1	1601.0	20.6	25.2	1.8 (0.7)	1.9 (1.0)	2.53 (0.72)	0.14
2	1633.6	33.1	59.9	35.2 (1.2)	46.7 (4.2)	1.66 (0.03)	−0.11
3	1651.8	39.3	45.2	56.0 (1.2)	45.6 (3.8)	2.73 (0.36)	0.18
4	1672.3	21.8	65.3	7.0 (1.3)	5.7 (0.5)	2.66 (0.41)	0.16

[a] Values in parentheses are mean deviations.

solution is greatly enhanced (though not guaranteed), and the gradient at most points in the χ^2 surface will be steeper, yielding greater precision for individual parameters.

In the present study, one simultaneous fit was performed on three unpolarized spectra for the transmission study, and a separate fit was performed on three pairs of parallel/perpendicular polarized spectra for the internal reflection study. Only the spectral region between 1750 and 1550 cm^{-1} was considered. Each spectrum was fit with the minimum number of bands sufficient to meet three criteria: (a) narrow uncorrelated residual amplitudes (fwhm < 10 cm^{-1}), (b) a ratio of spectral amplitudes to residual amplitudes that corresponded to the apparent signal:noise ratio of the original spectra, and (c) reduction of the χ^2 gradient to within 1 order of magnitude of single-precision arithmetic. Error estimates are discussed below.

Spectral dichroism was evaluated according to the two-phase approximation (*25*−*27*) (see Discussion). The order parameters, **S**, so derived pertain to the orientational order of the amide I vibrational transition moment; a value of **S** = 1.0 indicates a perfectly ordered system oriented perpendicular to the membrane surface, **S** = −0.5 indicates a perfectly ordered system oriented parallel to the membrane, and **S** = 0.0 indicates a system that may be perfectly disordered (isotropic), perfectly ordered and oriented at the magic angle (54.7° relative to the membrane normal), or a variety of more likely distributions. Since dichroic ratios were calculated only for band components with identical positions, widths, and shapes, they are equivalent whether calculated from component amplitudes or areas.

RESULTS

Transmission spectra of soluble annexin V in the absence of lipid were obtained in triplicate by alternately placing three samples of calcium-containing buffer, and three different 80 μg samples of annexin V in calcium-containing buffer, between two CaF_2 windows. The spectra exhibited absorption bands in the amide I region that could be well fit by a major component located at 1652.3 cm^{-1} and a minor (<1%) component at 1691.6 cm^{-1}; complete IRfit results are given in Table 1. Spectral results from samples that had not been dried and resuspended in D_2O were similar but exhibited more difficult baseline and noise problems. The amplitudes ranged from 33.7 to 34.4 milliabsorbance units, and the residual amplitudes after fitting corresponded to a signal: noise ratio of 47 (Figure 3). The baselines of these spectra were markedly tilted, as is common with transmission IR spectroscopy. Since IRfit only fits baselines that are flat and

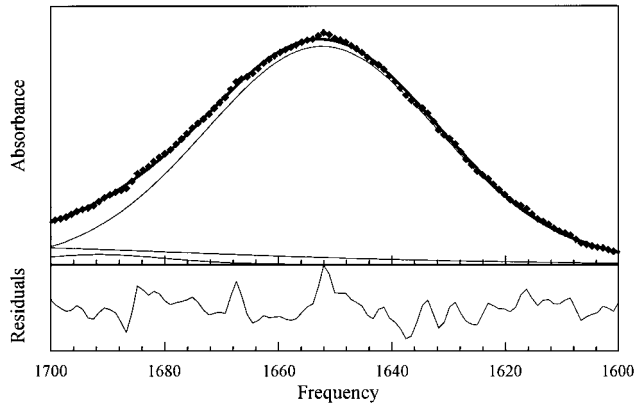

FIGURE 3: Transmission spectrum of soluble annexin V in calcium-containing lipid-free buffer. The spectroscopic data are represented by ◆; the three component bands recovered by IRfit are shown as thin solid lines, and their sum approximating the data is shown as a thick solid line. Residual amplitudes below are the difference between the data and the sum of the components. Residual peaks at 1652 and 1668 cm^{-1} are due to water vapor.

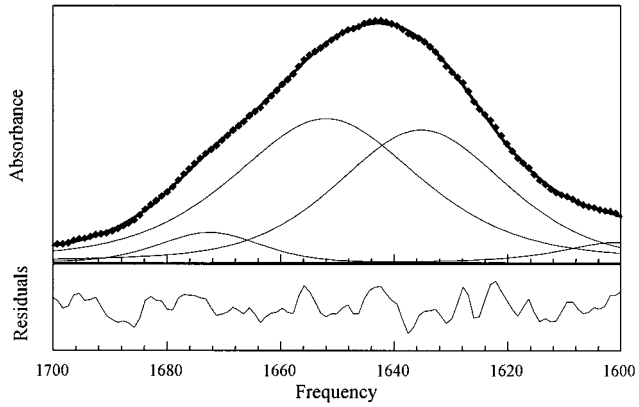

FIGURE 4: PATIR−FTIR spectrum of annexin V on a supported lipid monolayer; symbols and format as for Figure 3. In the absence of calcium in the subphase, no detectable absorption develops in this region, indicating that this spectrum is due solely to membrane-adsorbed protein.

level, tilted baselines are handled by adding an additional high-frequency broad band to the fitting solution such that one of the quasi-linear sloping wings of the band underlies the region of interest. In Figure 3, the low-frequency tail from such a band centered at ∼1800 cm^{-1} with a width of ∼350 cm^{-1} may be seen. The frequency, width, or shape parameters of these extreme bands were not linked across experiments. Peak residual amplitudes generally correspond to the characteristic absorption bands of H_2O vapor (e.g., 1652 and 1668 cm^{-1}). There was no detectable absorption in the amide II region, indicating that H → D exchange was effectively complete.

High-quality transmission spectra of annexin V in the presence of lipid vesicles could not be obtained. A minimum acceptable signal:noise ratio for transmission spectra in a 0.012−0.015 mm transmission cell required a minimum of 50 μg of protein in 25 μL of buffer. Inclusion of a 30-fold molar excess of lipid for annexin V binding adversely affected signal quality in both background and sample spectra, probably due to interactions between lipid vesicles and the CaF_2 windows that are altered when annexin V is present. Despite a poor signal:noise ratio and a severely tilted baseline, however, it was evident that the amide I shape and position for membrane-bound annexin V is significantly different from that of soluble membrane-free annexin V (not shown). There is a shift of the absorption maximum to lower frequencies, and new components appear at 1617 and 1675 cm^{-1}.

Internal reflection spectra of annexin V were recorded on a 1:1 DMPC/DMPS monolayer at a surface pressure of 25 dyn/cm. After injection of protein into the buffer subphase, no absorption signal develops for up to 3 h in the absence of calcium. This demonstrates that spectroscopic signals do not arise from annexin V in bulk solution. When sufficient calcium was added to make $[Ca^{2+}] = 1$ mM in the subphase, a clear amide I signal developed (Figure 4) and reached a plateau amplitude after approximately 2 h. There was no increase in membrane surface pressure during this period, indicating that the introduction of annexin V into the subphase did not lead to the insertion and lateral displacement of lipids in the membrane.

The amide I regions of the internal reflection spectra could not be adequately fit with a single major component, and multiple fits of equivalent apparent validity could be obtained when each spectrum was fitted individually. Linked analysis of three parallel and three perpendicular spectra yielded two major components at 1633.6 and 1651.8 cm^{-1}, two minor components, and a signal:residual noise ratio of 67 (Table 1). The overall dichroic ratio for amide I absorptions is 2.20 ($\mathbf{S} = 0.06$); the ratio for the component at 1633.6 cm^{-1} was 1.66 ($\mathbf{S} = -0.11$), and at 1651.8 cm^{-1} it was 2.73 ($\mathbf{S} = 0.18$). The isotropic dichroic ratio for this configuration is 2.0, corresponding to $\mathbf{S} = 0.0$, while $\mathbf{S} = 0.25$ for a sample that is uniformly oriented at a 45° angle. Thus, amide I vibrational transition moments in this protein as a whole exhibit a slight preference for an orientation perpendicular to the membrane surface. Those transitions giving rise to the band at 1633.6 cm^{-1} are ordered in the plane of the membrane to a substantially higher degree than those at 1651.8 cm^{-1}. Complete results from IRfit are summarized in Table 1.

These results required us to examine whether it is possible to resolve band components as close as 1633.6 and 1651.8 cm^{-1} and whether IRfit offers any advantage over other analytical methods operating on one spectrum at a time. This issue was addressed by using synthetic spectra. We generated three synthetic spectra comprising of two component bands at 1650 and 1635 cm^{-1}, each with a FWHM = 40 cm^{-1} and a shape that is 50% Gaussian. The amplitude of the 1635 cm^{-1} component was 80%, 70%, and 60% of the 1650 cm^{-1} component in the three spectra (designated S80, S70, and S60, respectively), and random noise with an amplitude corresponding to a signal:noise ratio of 50 (relative to the total amplitude) was added.

We attempted to recover the component bands from these spectra using several techniques. A single-component fit by the IRfit program of each spectrum individually yields a single band near 1643 cm^{-1}. S80, for example, yields a frequency of 1643.4 cm^{-1}, a FWHM of 45 cm^{-1}, a 67% Gaussian shape, and a signal:residual noise ratio of 36 (Figure 5A). Fourier self-deconvolution points to the presence of true bands at 1650 and 1635 cm^{-1} but also to the presence of false bands at 1620 and 1665 cm^{-1}. Second-derivative analysis is severely affected by the noise and does not suggest the presence of more than one band. Thus, we cannot resolve

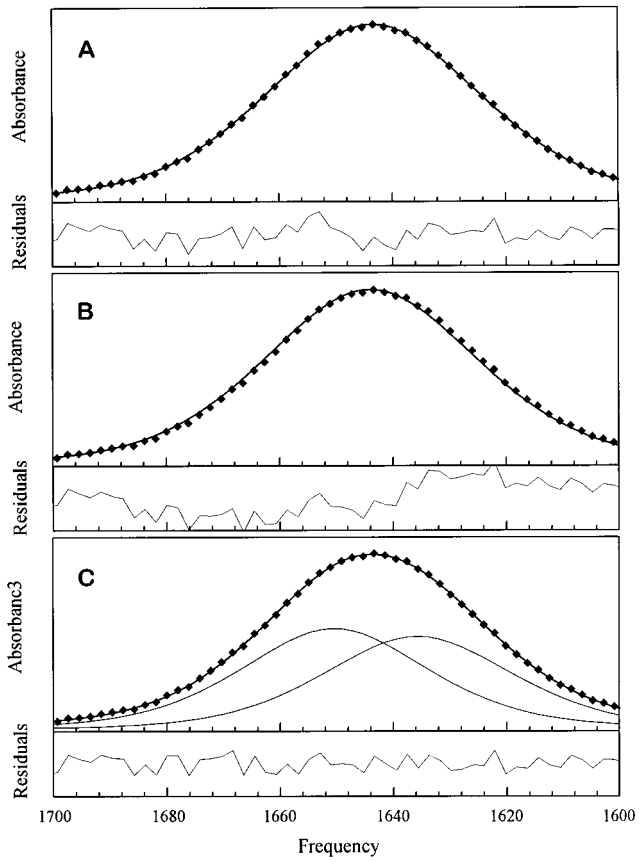

FIGURE 5: IRfit results for a synthetic spectrum composed of 2 component bands at 1650 and 1635 cm^{-1}, each with a FWHM = 40 cm^{-1}, and a shape that is 50% Gaussian. The amplitude of the 1635 cm^{-1} component was 80%, 70%, and 60% of the 1650 cm^{-1} component in the three spectra (S80, S70, and S60, respectively), and random noise with an amplitude corresponding to a signal: noise ratio of 50 (relative to the total amplitude) was added. (A) Results for an individual fit of S80. (B) Results for the fit of S80 when fit simultaneously with S70 and S60 and when only one fitted band is allowed. The presence of systematic variation in the residual amplitudes suggests that an additional component is required. (C) Results for the fit of S80 when fit simultaneously with S70 and S60 and two fitted bands are allowed. IRfit recovers the true components in all three synthetic spectra.

two bands with these frequencies, widths, and amplitudes in a single spectrum using these techniques.

A simultaneous linked analysis of all three spectra, however, clearly indicated that a single-component fit is inadequate. In Figure 5B, the results of fitting S80 simultaneously with S70 and S60 are shown; clear systematic variation in the residual amplitudes is apparent (this variation was also seen in S60 but was not apparent in the fit of S70). When a second band was permitted in the fitting solution, IRfit successfully recovered bands at 1650.5 and 1635.7 cm^{-1}, with FWHM of 39.7 and 40.2 cm^{-1} and shapes that were 54.7% and 58.7% Gaussian (Figure 5C). We conclude that linked analysis is able to resolve bands within 15 cm^{-1} of each other under conditions that may mimic some features of our experimental data and that this degree of resolution cannot be achieved when spectra are analyzed individually.

To estimate the dichroic behavior expected of membrane-bound annexin V, assuming that the crystal structure represents the membrane-bound form of annexin V, a computer model of the crystal structure of rat annexin V (*11*) was oriented such that the $x-y$ plane was the best-fit

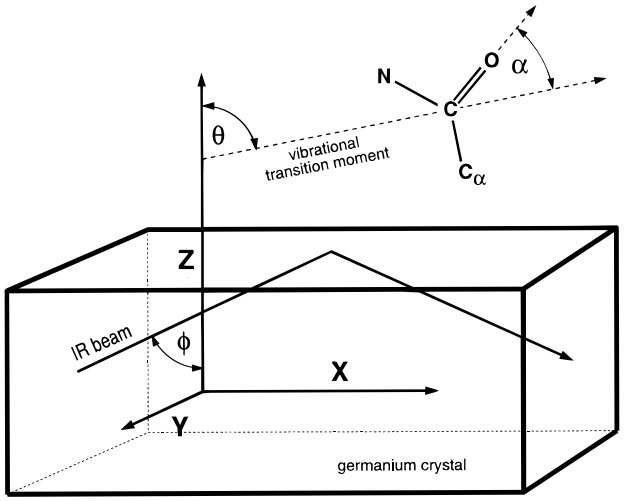

FIGURE 6: Coordinate conventions for PATIR−FTIR spectroscopy. The *x* axis is parallel to the long axis of the crystal support; the *z* axis is perpendicular to the supported membrane surface. α is the angle between the amide I vibrational transition moment, and θ is the angle this moment makes with the *z* axis. The angle of incidence between the infrared beam and the surface normal, ϕ, is 45° in this work.

plane through the bound calcium ions. For each peptide bond in this model, vectors representing the assumed transition moment were calculated to lie at an angle α from the carbonyl double bond, away from the peptide nitrogen, in the plane of the peptide bond (Figure 6). For each angle α, we calculated the corresponding value of cos θ (the projection of the normalized transition moment vector onto the *z* axis), and the expected value of the order parameter, *S*, according to

$$S' = \langle P_2(\cos\theta)\rangle = \frac{3}{2n}\left(\sum_i^n \cos^2\theta_i\right) - {}^1/_2$$

where θ_i is the angle between the amide I vector and the *z* axis (normal to the membrane surface) for residue *i* of *n* residues, primes indicate that the value is calculated from a crystal structure (rather than measured), and P_2 represents the second-order Legendre polynomial (*25*). Figure 7A shows the value of S' expected as a function of α for all residues in annexin V. Since values for α are believed to lie between 20°and 25° (*28*−*31*), these results lead us to expect values of 0.17−0.22 for the overall molecular order of annexin V. The same calculation performed separately for the helical and coil segments of annexin V predict order parameters of 0.22−0.28 for the helices and −0.01 to 0.03 for the coil segments (Figure 7B,C). For comparison with experimental values, these order parameters should be scaled by a factor representing the expected disorder of the support surface. In a prior investigation with a different silanized germanium crystal, this factor was found to be 0.82 (*25*).

DISCUSSION

Our results indicate that annexin V undergoes a conformational change upon binding to an anionic lipid membrane. The evidence takes two forms. First, there is a clear and large difference in the shape of the amide I absorption band for soluble versus membrane-bound annexin V (cf. Figures 3 and 4). Second, there is a significant quantitative difference

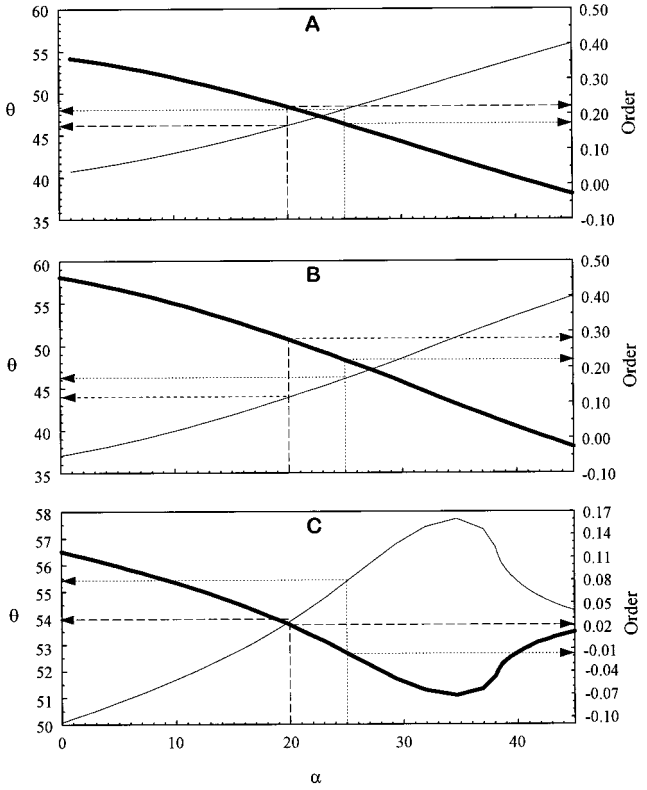

FIGURE 7: Relationship between α, θ, and predicted order parameter, S', for the annexin V crystal structure. Calculations were performed with a structure in which the seven calcium ions had been aligned as well as possible with the $x-y$ plane. The precise value of α in a protein is not known and must be assumed; these figures illustrate how uncertainty in the value of α translates nonlinearly into uncertainty about the molecular order. The thin solid line relates α to θ (left abscissa), and the thick solid line relates α to predicted order, S'. (A) All protein residues; (B) helical residues only; (C) nonhelical residues only.

between the overall measured dichroism of membrane-bound annexin V and the value predicted from the membrane-free crystal structure.

The change in amide I shape upon membrane binding consists of new absorbance components at 1635 and 1672 cm^{-1}, suggesting the presence of β-structure in the membrane-bound form, possibly antiparallel β-sheet. This evidence is seen in both the transmission spectra and the internal reflection spectra, although the latter are of considerably higher quality. While the crystal structure of annexin V is composed of approximately 74% helix and 26% random coil, whereas <55% of amide I absorption is attributable to α-helix in the membrane-bound form, we are reluctant to make quantitative predictions about the relative amounts of secondary structure present based on band area (although this is frequently done) because the extinction coefficient for amide I absorption is a sensitive function of secondary structure (*32*). Moreover, any spectral component we attribute to α-helix can be heterogeneous, with contributions from nonhelical structures leading to an overestimate of helix.

It may be possible for the 1635 cm^{-1} component we observe to arise from annexin-induced perturbation of the α-carboxylate group of DMPS. However, we consider this unlikely because α-carboxylate groups tend to absorb at lower frequencies (*33*), it would not explain the concomitant appearance of a component at 1672 cm^{-1}, and there is an increase in signal at 1635 cm^{-1} in *both* polarizations. The latter would not occur if annexin merely induced reorientation of the seryl α-carboxylate. The use of DMPS with a ^{13}C-labeled carboxylate would be necessary to completely eliminate the possibility of the 1635 cm^{-1} component arising from a heretofore unrecognized vibrational mode peculiar to the ternary protein−calcium−lipid complex.

The measured overall order parameter for the amide I vibrational transition moment of membrane-bound annexin V is $S = 0.06$, whereas we predict $S' = 0.17-0.22$ on the basis of a reasonable orientation of the crystal structure with respect to a membrane surface. These values are significantly different and remain so even after allowing for a reasonable amount of disorder due to crystal surface roughness (e.g., by a factor of 0.82) (*25*). This difference appears to be due to significant amounts of β structure in membrane-bound annexin V, for which the transition moments are ordered parallel to the membrane surface ($S = -0.11$, Table 1). Signals arising from this β structure may be disproportionately represented in the overall signal due to relatively large extinction coefficients (*32*). We find much better quantitative agreement between an order parameter calculated for the spectral feature we attribute to α-helix ($S = 0.18$ for the band at 1651.8 cm^{-1}, Table 1) and the transition order expected from helices in the crystal structure ($S' = 0.22-0.28$), especially if we scale the latter to account for disorder due to surface roughness in the experimental measurements.

Thus, our results are consistent with evidence from electron microscopy indicating that the domain structure of annexin V is preserved with only slight changes upon membrane binding that render the calcium binding sites roughly coplanar (*18, 34*). They contrast with those of a far-UV circular dichroism study indicating that annexin V does not undergo a significant conformational change upon binding to lipid vesicles (*35*). However, this study examined only wavelengths between 205 and 240 nm, whereas the majority of signals specifically arising from β structure are observed at <205 nm. Therefore, this study could well miss the formation of β structure. Indeed, the slight decrease in ellipticity at 222 nm found in this study upon addition of lipid vesicles is consistent with our suggestion that nonhelical structures must emerge (presumably at the expense of helical structure) under these conditions.

On the basis of X-ray crystallographic results (*18*), we infer that the most likely site for annexin V to undergo conformational change upon membrane binding involves the segments linking domains I/IV and II/III. Inspection of the crystal structure shows these linking segments to be only long enough to span the distance between helices. Various residue side chains situated between the domains require the planes defined by the calcium binding sites in each domain to tilt (Figure 1B). To align these planes in the manner suggested by electron microscopy, the helices must unravel to some degree. We speculate that residues in these linking segments, and a portion of those in the helices to which they attach, are recruited into β structure upon membrane binding. However, our spectroscopic data cannot localize the conformational change to any segment or domain of the protein, and the images provided by electron microscopy are not of sufficient resolution to support or refute this speculation.

From the negative order parameter recovered for the band component at 1633 cm^{-1}, we infer that the β structure formed must be oriented such that the transverse axis (roughly

corresponding to the interstrand hydrogen bonds) is oriented parallel to the membrane surface (i.e., the $x-y$ plane; see Figure 6). The spectroscopic data do not constrain the orientation of the longitudinal axis (corresponding to the direction of the backbone chain); the data are consistent with a longitudinal axis that is perpendicular, tilted, or even parallel to the membrane surface (*36*). If the longitudinal axis is oriented parallel to the membrane, however, then the transverse axis is very limited in the ways in which it can situate parallel to the surface, whereas the transverse axis may assume any orientation in the $x-y$ plane if the longitudinal axis is perpendicular (*37*).

Order parameters in this work were calculated by using only the so-called two-phase approximation for calculating electric field amplitudes in the evanescent field (*38*). Annexin V clearly adsorbs to the membrane surface, but the association is superficial (*39*); our Langmuir results also indicate that it does not insert and displace membrane lipids laterally. Since the protein resides in the bulk aqueous phase, questions about how to calculate the amplitudes of electric field components *within the membrane* are irrelevant (*26*, *27*, *40*), and use of the thin-film approximation is inappropriate. Moreover, attempts to calculate electric field amplitudes based on an assumption about the refractive index *within the protein* are confounded by anomalous dispersion at the frequencies of interest. Nonetheless, even if the thin-film approximation were applied to our results, it would merely reduce the transition order for dichroic ratios less than 2.0 and increase the apparent helix order from 0.18 to 0.32, not substantially changing our conclusions.

The experiments we have reported were performed by recording background spectra with the lipid membrane already on the crystal. Thus, absorption bands arising from the lipid are not seen in the final spectra, and we cannot directly address any effects that annexin V may exert on the membrane. However, we do not see positive or negative bands, or derivative-like features where lipid bands characteristically absorb, that would indicate a spectral change upon annexin binding. NMR spectroscopy appears to yield mixed information about whether annexin binding causes structural changes in the lipids of small unilamellar vesicles (*35*, *41*). It remains possible that our results would differ if we examined annexin V binding to bilayers or monolayers at the air−water interface, since supported lipid monolayers may exhibit less mechanical yield than unsupported lipid bilayers or monolayers. However, it was reasonable to focus on supported monolayers in this study since the studies of annexin V by electron microscopy were also performed on supported monolayers.

We have introduced a novel approach to PATIR−FTIR spectroscopy and spectral analysis in this paper. The spectrometer configuration used in this work differs from that described previously (*23*) in that the silane-treated crystal is applied flat onto the monolayer (Figure 2). This technique has proven to be more reproducible than the Langmuir−Blodgett technique formerly used, and more sensitive since there are 12 internal reflections rather than 7. It is clear that PATIR−FTIR spectroscopy is advantageous for the study of membrane-bound proteins not only because it yields information about orientational order but also because of dramatically enhanced sensitivity. Transmission studies of membrane-bound protein required 80 μg of protein concentrated in a volume of 20 μL and yielded marginal signal quality, whereas the internal reflection studies were performed with 20 μg aliquots of protein injected into a subphase volume of 6 mL and yielded excellent signal quality. Another significant advantage of the internal reflection spectra is that they generally require no correction for tilted baseline.

Linked analysis borrows directly from an approach known as "global analysis" that has become popular in the field of fluorescence intensity decay analysis (*20*, *21*). In its current form, IRfit is considerably less ambitious than fluorescence global analysis, being limited to simultaneous fitting of identical experiments or to spectra collected with different polarizer orientations wherein only amplitude changes are to be expected. We have not yet defined a role for the global analysis of infrared spectra obtained under changing physical or chemical circumstances that may also change the frequency, width, and shape of an infrared absorption. Nonetheless, linked analysis has obvious and important advantages even within this relatively circumscribed application.

Linked analysis is advantageous for helping to (a) reduce the amount of subjective input involved in the analysis of infrared spectra and (b) avoid overanalysis. Traditional approaches to infrared analysis (i.e., bandfitting) generally require the investigator to estimate all initial parameter values. The results of these methods can differ greatly depending on which initial values are chosen or on the order in which they are chosen. Techniques such as Fourier self-deconvolution (*42*−*47*) and second-derivative analysis (*48*, *49*) also attempt to reduce subjectivity in spectral analysis but can be thwarted by even modest amounts of noise in the spectra. Even when noise does not limit their application, however, subjectivity is still involved when deciding how much deconvolution is appropriate, and how many of the apparent bands to include in the fit. When applied uncritically, these techniques lead to the inclusion of superfluous components in the fitting procedure and nonunique solutions—two hallmarks of overanalysis.

Linked analysis also requires one to provide initial estimates for all parameter values used; however, subjectivity is reduced in two ways: First, many of the parameters are applied uniformly to multiple spectra. This reduces the number of independent parameter value estimates that must be input into the program, thereby increasing the ratio of data:parameters, imparting more information content to each parameter, and steepening the multidimensional χ^2 surface (i.e., it overdetermines each parameter, narrowing the local χ^2 minima and increasing the precision of the recovered parameter value). Second, all parameters are allowed to float unconstrained during the fitting procedure. This is not possible in standard approaches when one spectrum at a time is fitted because separate analyses often lead to differences in the frequency, width, or shape of recovered components. Because the spectral components for which a dichroic ratio is to be calculated should have the same frequency, width, and shape, allowing parameters to float freely would generally thwart the analysis of infrared dichroism.

Since linked analysis reduces the number of parameters used to fit the data, the likelihood of obtaining a unique fit, while not guaranteed, is greatly enhanced. We cannot be certain that individual components recovered by linked analysis map to physically distinct entities, but efforts to

develop a reliable mapping between features of the spectra and of proteins are likely to be aided by means to extract unique and relatively objective solutions. Another significant advantage of simultaneous linked analysis over the analysis of individual spectra is that it makes possible the detection and recovery of component bands that are otherwise not resolvable. This advantage is most likely to be gained when components in the absorption spectra differ in relative amplitudes, as to be expected when the polarization is changed. However, circumstances may well arise wherein relative amplitudes are the same regardless of polarization, and it may not be possible for these bands to be resolved by linked analysis.

One concern raised about linked analysis is that it yields a single-valued result for most parameters and no estimate for the uncertainty in their value. This is true for the frequency, width, and shape parameters in the work presented in this paper. However, there is no requirement for precision in these values. Rather, the overriding requirement is for consistency in their value between experiments. Linked analysis yields this consistency, yet while providing independent component amplitude results that may then be subjected to ordinary error analysis. For future experiments in which the precision of other parameters may be important, software developments are planned to permit driving selected parameter values away from their minima, and enable a rigorous statistical evaluation of the consequences. In fluorescence intensity decay analysis, this approach has been used to define the range of statistically indistinguishable values for each parameter and to escape from statistically insignificant local minima on a multidimensional χ^2 surface (*21*).

SUMMARY

There is a clear conformational difference between soluble annexin V, as characterized by transmission IR spectroscopy, and membrane-bound annexin V, as characterized by transmission and internal reflection IR spectroscopy. Our results suggest that some β structure is formed upon binding to a membrane and that this β structure is oriented so that interstrand hydrogen bonds are oriented parallel to the membrane surface. We interpret these results as consistent with, and complementary to, earlier studies conducted by others using X-ray crystallography, electron microscopy, and circular dichroism spectroscopy.

We found linked analysis to be advantageous for the analysis of these spectral results. In tests on synthetic spectra of known composition and similar shape, it is clear that linked analysis improves both the sensitivity and the accuracy of component recovery. While we cannot know a priori how many components are present in the amide I region of any given spectrum, simultaneous linked analysis of multiple spectra is more likely to yield a unique, more objective, and internally consistent quantitative analysis of amide I absorption bands than traditional analytical methods applied to individual spectra.

ACKNOWLEDGMENT

We are grateful to Richard Mendelsohn and Barbara Seaton for comments on a preliminary version of this manuscript.

REFERENCES

1. Creutz, C. E. (1992) *Science 258*, 924−931.
2. Swairjo, M. A., and Seaton, B. A. (1994) *Annu. Rev. Biophys. Biomol. Struct. 23*, 193-213.
3. Demange, P., Voges, D., Benz, J., Liemann, S., Gottig, P., Berendes, R., Burger, A., and Huber, R. (1994) *Trends Biochem. Sci. 19*, 272−276.
4. Liemann, S., and Lewit-Bentley, A. (1995) *Structure 3*, 233−237.
5. Mollenhauer, J. (1997) *Cell. Mol. Life Sci. 53*, 506−507.
6. Huber, R., Romisch, J., and Paques, E. P. (1990) *EMBO J. 9*, 3867−3874.
7. Huber, R., Berendes, R., Burger, A., Schneider, M., Karshikov, A., Luecke, H., Romisch, J., and Paques, E. (1992) *J. Mol. Biol. 223*, 683−704.
8. Weng, X., Luecke, H., Song, I. S., Kang, D. S., Kim, S. H., and Huber, R. (1993) *Protein Sci. 2*, 448−458.
9. Sopkova, J., Renouard, M., and Lewit-Bentley, A. (1993) *J. Mol. Biol. 234*, 816−825.
10. Bewley, M. C., Boustead, C. M., Walker, J. H., Waller, D. A., and Huber, R. (1993) *Biochemistry 32*, 3923−3929.
11. Concha, N. O., Head, J. F., Kaetzel, M. A., Dedman, J. R., and Seaton, B. A. (1993) *Science 261*, 1321−1324.
12. Burger, A., Berendes, R., Liemann, S., Benz, J., Hofmann, A., Gottig, P., Huber, R., Gerke, V., Thiel, C., Romisch, J., and Weber, K. (1996) *J. Mol. Biol. 257*, 839−847.
13. Benz, J., Bergner, A., Hofmann, A., Demange, P., Gottig, P., Liemann, S., Huber, R., and Voges, D. (1996) *J. Mol. Biol. 260*, 638−643.
14. Liemann, S., and Huber, R. (1997) *Cell. Mol. Life Sci. 53*, 516−521.
15. Newman, R. H., Leonard, K., and Crumpton, M. J. (1991) *FEBS Lett. 279*, 21−24.
16. Brisson, A., Mosser, G., and Huber, R. (1991) *J. Mol. Biol. 220*, 199−203.
17. Driessen, H. P., Newman, R. H., Freemont, P. S., and Crumpton, M. J. (1992) *FEBS Lett. 306*, 75−79.
18. Voges, D., Berendes, R., Burger, A., Demange, P., Baumeister, W., and Huber, R. (1994) *J. Mol. Biol. 238*, 199−213.
19. Tatulian, S. A., Biltonen, R. L., and Tamm, L. K. (1997) *J. Mol. Biol. 268*, 809−815.
20. Knutson, J. R., Beechem, J. M., and Brand, L. (1983) *Chem. Phys. Lett. 102*, 501−507.
21. Axelsen, P. H., Bajzer, Z., Prendergast, F. G., Cottam, P. F., and Ho, C. (1991) *Biophys. J. 60*, 650−659.
22. Bartlett, G. R. (1959) *J. Biol. Chem. 234*, 466−468.
23. Axelsen, P. H., Braddock, W. D., Brockman, H. L., Jones, C. M., Dluhy, R. A., Kaufman, B. K., and Puga, F. J. I. (1995) *Appl. Spectrosc. 49*, 526−531.
24. Press, W. H., Flannery, B. P., Teukolsky, S. A., and Vetterling, W. T. (1986) in *Numerical Recipes*, Cambridge University Press, Cambridge, England.
25. Axelsen, P. H., Kaufman, B. K., McElhaney, R. N., and Lewis, R. N. A. H. (1995) *Biophys. J. 69*, 2770−2781.
26. Axelsen, P. H., and Citra, M. J. (1997) *Prog. Biophys. Mol. Biol. 66*, 227−253.
27. Citra, M. J., and Axelsen, P. H. (1996) *Biophys. J. 71*, 1796−1805.
28. Abbott, N. B., and Elliott, A. (1956) *Proc. R. Soc. (London) A 205*, 247−268.
29. Miyazawa, T., and Blout, E. R. (1961) *J. Am. Chem. Soc. 83*, 712−719.
30. Ambrose, E. J., and Elliott, A. (1951) *Proc. R. Soc. (London) A 205*, 47−61.
31. Fraser, R. D. B. (1953) *J. Chem. Phys. 21*, 1511−1515.
32. de Jongh, H. H., Goormaghtigh, E., and Ruysschaert, J. M. (1996) *Anal. Biochemistry 242*, 95−103.
33. Venyaminov, S. Y., and Kalnin, N. N. (1990) *Biopolymers 30*, 1243−1257.
34. Brisson, A., Mosser, G., and Huber, R. (1991) *J. Mol. Biol. 220*, 199−203.
35. Swairjo, M. A., Roberts, M. F., Campos, M. B., Dedman, J. R., and Seaton, B. A. (1994) *Biochem. 33*, 10944−10950.
36. Marsh, D. (1997) *Biophys. J. 72*, 2710−2718.

37. Wimley, W. C., Hristova, K., Ladokhin, A. S., Silvestro, L., Axelsen, P. H., and White, S. H. (1998) *J. Mol. Biol. 277*, 1091−1110.
38. Harrick, N. J. (1967) in *Internal Reflection Spectroscopy*, Harrick Scientific Corporation, Ossining, NY.
39. Ravanat, C., Torbet, J., and Freyssinet, J. M. (1992) *J. Mol. Biol. 226*, 1271−1278.
40. Picard, F., Buffeteau, T., Desbat, B., Auger, M., and Pezolet, M. (1998) *Biophys. J. 74*, A313.
41. Saurel, O., Cezanne, L., Milon, A., Tocanne, J. F., and Demange, P. (1998) *Biochemistry 37*, 1403−1410.
42. Kauppinen, J. K., Moffatt, D. J., Mantsch, H. H., and Cameron, D. G. (1981) *Appl. Spectrosc. 35*, 271−276.
43. Kauppinen, J. K., Moffatt, D. J., Mantsch, H. H., and Cameron, D. G. (1981) *Anal. Chem. 53*, 1454−1457.
44. Kauppinen, J. K., Moffatt, D. J., Hollberg, M. R., and Mantsch, H. H. (1991) *Appl. Spectrosc. 45*, 411−416.
45. Mantsch, H. H., Moffatt, D. J., and Casal, H. L. (1988) *J. Mol. Struct. 173*, 285−298.
46. Surewicz, W. K., and Mantsch, H. H. (1988) *Biochim. Biophys. Acta 952*, 115−130.
47. Byler, D. M., and Susi, H. (1986) *Biopolymers 25*, 469−487.
48. Singh, B. R., Wasacz, F. M., Strand, S., Jakobsen, R. J., and DasGupta, B. R. (1990) *J. Protein Chem. 9*, 705−713.
49. Lee, D. C., Hayward, J. A., Restall, C. J., and Chapman, D. (1985) *Biochemistry 24*, 4364−4373.

BI981289O